

Caffeine removal and mass transfer in a nanofiltration membrane process

Samantha Jeffery-Black^a, Steven J. Duranceau^{a,*}, Carolina Franco^b

^aDepartment of Civil, Environmental, and Construction Engineering, University of Central Florida, P.O. Box 162450, Orlando, FL 32816-2450, USA, Tel. 407-823-1440; Fax: 407-823-3315; email: steven.duranceau@ucf.edu

^bDepartment of Chemistry, University of Central Florida, Orlando, FL 32816-2450, USA

Received 22 September 2016; Accepted 20 October 2016

ABSTRACT

The effectiveness of nanofiltration (NF) to remove a wide range of spiked caffeine (0.052–4,500 µg/L) from groundwater at the pilot-scale (60,636 L/h) has been demonstrated. Experiments were conducted using a pilot-scale unit, operating as a two-stage, split-feed, center-exit system that relied on a well supply withdrawn from an average depth of 45 m that contained an average of 11 mg/L of dissolved organic carbon. The average caffeine removal efficiency across the pilot system was 68%, and removal did not vary by solute concentration for constant flux (25.6 L m⁻² h⁻¹) and temperature (25°C) operating conditions. Mass transfer models evaluated in this work include the homogeneous solution diffusion model (HSDM) with and without film theory (FT), in addition to dimensional analysis, using the Sherwood number, and were shown to predict NF solute mass transfer. Predicted vs. actual caffeine content was linearly compared, revealing correlation coefficients on the order of 0.99, 0.96, and 0.99 for the HSDM without FT, HSDM-FT, and the Sherwood number, respectively. However, the use of the HSDM-FT and the Sherwood number resulted in the over-prediction of caffeine concentrations in permeate streams by 27% and 104%, respectively.

Keywords: Solution diffusion model; Mass transfer coefficient; Sherwood number; Dimensional analysis

1. Introduction

Trace organic compounds (TrOCs), including endocrine disrupting compounds, pharmaceuticals, personal care products, and pesticides, are of growing concern due to their relatively recent detection in the aquatic environment. TrOCs typically make their way into the environment via wastewater effluent discharge to rivers and streams, in addition to wastewater reclamation for irrigation. Consequently, these compounds have been detected in drinking water sources with concentrations up to the parts per billion (ppb) level [1–3].

Research has shown that TrOCs can be effectively removed by certain membrane technologies, including nanofiltration (NF) and reverse osmosis (RO) processes [4–8]. The extent of TrOC removal is dependent on many

factors, including solute properties (size, charge, hydrophobicity, geometry, etc.), membrane type (molecular weight cut off [MWCO], pore size) and operation (flux, recovery), and feed water quality characteristics (pH, ionic strength, organic content) [9–15].

Several models have been used to predict NF membrane performance. Many originate from the extended Nernst–Planck equation, first proposed by Schlogl [16], including the Donnan–Steric-pore model (DSPM) originally proposed by Bowen et al. [17] that was later adapted to include a dielectric effect (DSPM&DE) [18]. These models incorporate diffusion, convection, and electrostatic interactions that occur between charged compounds and membranes. The extended Nernst–Planck equation was originally used to describe the transport of electrolytes in RO through ion exchange membranes, and takes into consideration the ionic flux, solvent velocity, and hindrance factors to account for both convection and diffusion [19]. The extended

*Corresponding author.

Nernst–Planck equation is often modified and improved to enhance the prediction of rejection by membranes, such as in the case of film theory (FT) [20,21].

Regardless, the DSPM&DE is based on the extended Nernst–Planck equation and has proven success in predicting the rejection of inorganic salts although NF often over-predicts the rejection of organic compounds due to interactions with hydrophobic membranes [22]. To apply the DSPM&DE, three parameters must be known: the average pore size, effective thickness, and surface charge density of the membrane. These parameters are predetermined by model fitting the rejection data for simple probe solutes by the membrane [21]. Kong et al. [23] evaluated the DSPM&DE for the prediction of haloacetic acids and six neutral pharmaceuticals and found that while this model accurately predicted the rejection of haloacetic acids, pharmaceutical rejection was over-predicted.

Another widely used means to predict the performance of diffusion-controlled membrane water treatment processes has been the homogeneous solution diffusion model (HSDM) [24–27] and has been applied to TrOC modeling [4, 27–30]. Zhao and Taylor [24] created a diffusion-controlled model that incorporates the effects of water quality and time to predict solute mass transfer. Similarly, Zhao et al. [25] predicted permeate water quality using stage specific solute mass transfer coefficients in RO and NF processes. In their work, the HSDM was used with and without FT [25]. These concepts were supported by Hung et al. [26], who established a mass transfer model to predict water and salt transport through a RO process. They found that salt transport was governed through a solution-diffusion mechanism, while water transport was influenced by pressure.

The use of the HSDM has also been applied in the optimization of NF for the treatment of dyes and other synthetic chemicals in textile plant effluent by Shaaban et al. [31]. Duranceau [4] studied the removal of six synthetic organic compounds (SOC) from a NF pilot and used the HSDM to predict SOC removal. Verliefe et al. [27] used the solution-diffusion model to evaluate the rejection of neutral organics from NF membranes. Hidalgo et al. [28] used the solution diffusion model to predict atrazine in the permeate of four NF membranes, and Hidalgo et al. [29] used the HSDM to predict aniline removal from RO processes. The solution diffusion model can be modified by FT (HSDM-FT) to account for concentration polarization effects [25,27].

The purpose of this work was to predict the transport of an anthropogenic solute, caffeine, through a NF membrane process using two previously established diffusion-based models: the HSDM and the HSDM-FT. Diffusion-based models were selected based on their successful use in the prediction of NF performance by others [4,20,21,31] and the simplicity of obtaining desired mass transfer coefficients. This paper compares actual with predicted permeate stream caffeine concentrations for a two-stage NF pilot operating in a manner that simulates an adjacent full-scale plant process. Caffeine mass transfer coefficients were determined experimentally using linear regression and by using the Sherwood number correlation method, and these values were compared. The model was validated using results reported herein, as well as use of outside independent literature sources.

2. Theory

Diffusion-based models have proven to be valid tools for describing transport in diffusion-controlled membrane processes [4,25,28,29]. One of the more popular transport models, the HSDM, assumes solutes permeate through membranes in three steps: (1) solutes partition into the polymeric membrane on the feed side, (2) solutes diffuse through the bulk portion of the membrane, and (3) solutes partition completely through the membrane and into the permeate stream [32]. Incorporating FT into the HSDM accounts for possible effects of concentration polarization [25].

Eqs. (1)–(4) are commonly used in mass and flow balance calculations. Q_f , Q_p , and Q_c are the feed, permeate, and concentrate flow rates, respectively; C_f , C_p , and C_c are the feed, permeate, and concentrate concentrations, respectively; and R is the water recovery. These parameters are depicted graphically in a simplified membrane schematic, illustrated in Fig. 1.

$$Q_f = Q_p + Q_c \quad (1)$$

$$Q_f C_f = Q_p C_p + Q_c C_c \quad (2)$$

$$R = \frac{Q_p}{Q_f} * 100 \quad (3)$$

$$\text{Rejection} = \frac{C_f - C_p}{C_f} * 100 \quad (4)$$

Water flux, F_w , is the term used to describe the flow of water per unit of membrane area, and is calculated using Eq. (5), where A is the membrane area. The osmotic pressure, $\Delta\pi$, is the pressure that must be overcome to push water from the feed to the permeate and concentrate sides of the membrane. The transmembrane pressure differential, ΔP , is the pressure drop across the membrane, determined by calculating the average pressure between the feed and concentrate sides of the membrane. Consequently, the net applied pressure can be calculated as the transmembrane pressure differential minus the osmotic pressure differential [33]. K_w is the water mass transfer coefficient describing the water flux per unit of pressure and is experimentally determined using Eq. (5):

$$F_w = K_w(\Delta P - \Delta\pi) = \frac{Q_p}{A} \quad (5)$$

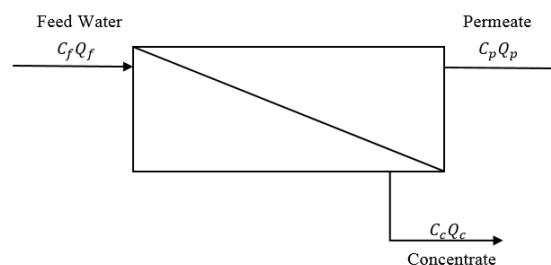


Fig. 1. Membrane schematic.

While water flux and water mass transfer coefficients are highly dependent on pressure, solute flux (F_s) and solute mass transfer coefficients (K_s) are controlled by diffusion [25]. The solute flux describes the throughput of a solute through a membrane process and is calculated using Eq. (6), where C_m is the concentration at the membrane surface and is calculated using Eq. (7).

The solute mass transfer coefficient is assumed to be constant for a specific solute, but can vary with water quality, operating conditions, and membrane properties [25,34]. The mass transfer coefficient for caffeine, K_s , can be determined experimentally by finding the slope between the solute flux and the change in solute concentration as demonstrated by Eq. (6), or by applying a Sherwood number correlation method utilizing Eqs. (9)–(13).

$$F_s = K_s(C_m - C_p) = \frac{Q_p C_p}{A} \quad (6)$$

$$C_m = \frac{C_f + C_c}{2} \quad (7)$$

The solute back-transport mass transfer coefficient, k_b , is determined using Eq. (8), and takes into account the concentration polarization effects describing the build-up of solutes at the feed side of the membrane surface due to partial rejection of these solutes [35].

$$\frac{C_m - C_p}{C_f - C_p} = \exp\left(\frac{F_w}{k_b}\right) \quad (8)$$

The Sherwood number is calculated using Eq. (9), assuming laminar flow conditions, where R_e is the Reynolds number, S_c is the Schmidt number, d_h is the hydraulic diameter (ft), L is the membrane channel length (ft), μ is the solution viscosity (kg/m/s), ρ is the density of water (kg/m³), D_i is the diffusivity of a species (m²/s), and V is the feed channel velocity (m/s). D_i is the Wilke–Chang correlation, calculated using Eq. (12), where ϕ is solvent association factor (2.26 for water), MW is the solute molecular weight (g/mole), T is the water temperature (K), and V_i is the solute molar volume at normal boiling point (m³/kmol), calculated by adding the individual solute atomic volumes [4,36–39].

$$S_h = 1.86 \left(R_e S_c \frac{d_h}{L} \right)^{0.33} \quad (9)$$

$$R_e = \frac{d_h V \rho}{\mu} \quad (10)$$

$$S_c = \frac{\mu}{\rho D_i} \quad (11)$$

$$D_i = \frac{(117.3 \times 10^{-15}) [(\phi)(MW)]^{0.5} (T)}{\mu V_i^{0.6}} \quad (12)$$

Once the Sherwood parameters are known, K_s can be determined using Eq. (13):

$$K_s = \frac{S_h D_i}{d_h} \quad (13)$$

Combining and rearranging Eqs. (1)–(7) results in Eq. (14), which is used to predict permeate concentration based on the HSDM. Adding the solute back-transport mass transfer coefficient into Eq. (14) results in the HSDM-FI, presented as Eq. (15). To use Eqs. (14) and (15), water and solute mass transfer coefficients, assumed to be constant, must be determined [25,40].

$$C_p = \frac{K_s C_f}{K_w (\Delta P - \Delta \pi) \left(\frac{2-2R}{2-R} \right) + K_s} \quad (14)$$

$$C_p = \frac{K_s C_f \exp\left(\frac{F_w}{k_b}\right)}{K_w (\Delta P - \Delta \pi) \left(\frac{2-2R}{2-R} \right) + K_s \exp\left(\frac{F_w}{k_b}\right)} \quad (15)$$

3. Materials and methods

3.1. Site description

This research was conducted using a 267-gallon per minute (gpm) NF pilot unit housing NF270 membranes (DOW Filmtec), owned and operated by the Town of Jupiter (Town) Water Utility. Jupiter is located along the southeast coast of Florida, and the water treatment facility serves approximately 80,000 customers over an area of 58 square miles. Their full-scale plant has a treatment capacity of 30 million gallons per day (MGD), utilizing RO, NF, and anion exchange processes in parallel. The NF plant was constructed in 2010 and has a maximum production capacity of 14.5 MGD.

3.1.1. NF pilot unit

The pilot and full-scale processes are uniquely configured: feed water is split prior to entering both the left and right sides of the six-element pressure vessels, then permeate is collected on both ends, while concentrate is collected in the center of the vessel, after only three membranes. A simplified schematic of the pretreatment system and unique membrane configuration is illustrated in Fig. 2. This configuration has resulted in a lower pressure drop between stages, since the water path only flows through half of the number of membranes compared with a typical NF plant.

Pilot specifications and operating parameters are presented in Table 1. Membrane elements in the pilot unit are the same as those currently employed by the Town's full-scale NF plant. The membranes are 8" in diameter and have a surface area of 400 ft². There are a total of 54 elements in the pilot, with 42 in the first stage and 12 in the second stage, and 6 elements per pressure vessel, forming a 7:2 array. This results in a total membrane area of 21,600 ft² in the pilot unit. The NF pilot operates with a feed flow rate of 267 gpm, resulting in a permeate flow rate of 226 gpm while operating at an 85% water recovery. The typical feed pressure of the pilot unit is 57 pounds per square inch (psi), while the permeate pressure is 21 psi.

3.1.2. Feed water quality

The Town's NF plant, and subsequently the Town's NF pilot unit, draws raw water from a fresh surficial ground

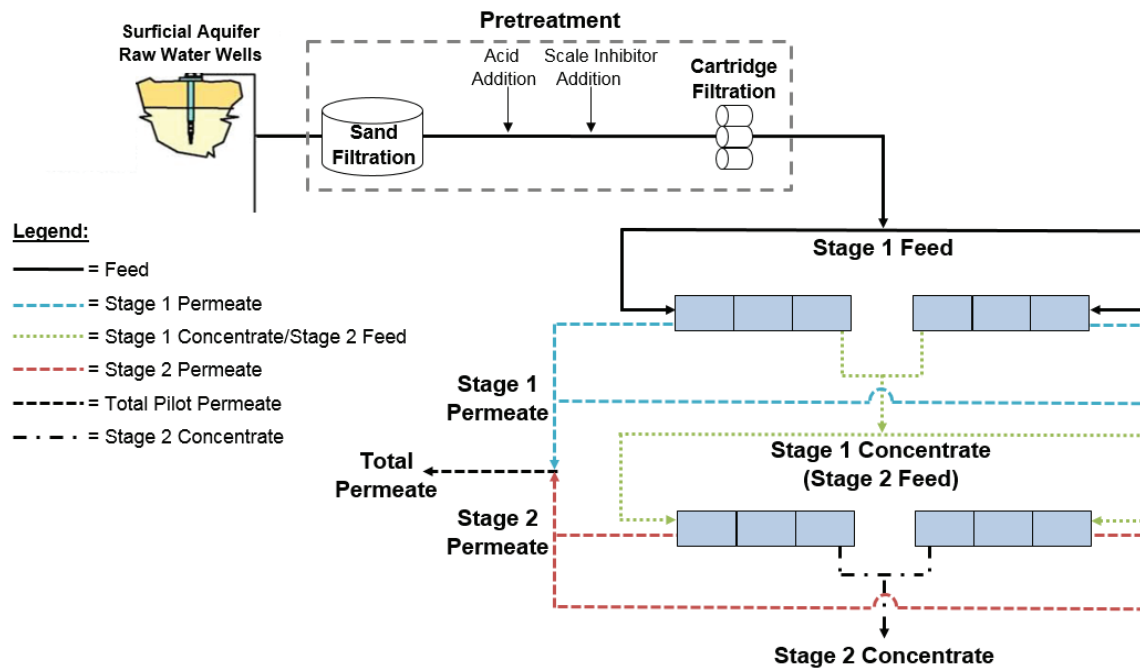


Fig. 2. Simplified schematic of NF pretreatment and flow configuration.

Table 1
NF pilot unit specifications and operating parameters

Item	Value	
Membrane module	NF270 (DOW Filmtec)	
Membrane composition	Polyamide thin-film composite	
MWCO (Da)	200–400	
Membrane pore diameter (nm) [41]	0.84	
MgSO ₄ and CaCl ₂ Rejection (%) [42]	97 and 40–60	
Pilot recovery (%)	85	
Total number of membrane elements	54	
Elements in stages 1 and 2	42 and 12	
Membranes per pressure vessel	6	
Array	7:2	
Membrane surface area (DOW Filmtec)	372 m ² /element	400 ft ² /element
Total membrane area in pilot	2,007 m ²	21,600 ft ²
Feed velocity	0.043 m/s	0.14 ft/s
Feed flow rate	60,636 L/h	267 gpm
Permeate flow rate	51,552 L/h	227 gpm
Concentrate flow rate	9,084 L/h	40 gpm
Feed pressure	3.93 bar	57 psi
Permeate pressure	1.45 bar	21 psi
Water flux	25.6 L m ⁻² h ⁻¹	15.1 gsf/d

Table 2
NF pilot water quality in feed and permeate samples

Water quality parameter	Units	Feed water	Total pilot permeate
pH	N/A	6.5	6.3
Temperature	°C	25	25
Conductivity	µS/cm	750	500
TDS	mg/L	455	250
Alkalinity	mg/L as CaCO ₃	240	172
Color*	Color units (CU)	45	<5
UV ₂₅₄	cm ⁻¹	0.406	0.06
DOC*	mg/L	11	<0.25
Chloride	mg/L	50	50
Calcium	mg/L	125	66
Sodium	mg/L	23	19

*Method detection limits for color and DOC are 5 CU and 0.25 mg/L, respectively.

water source. Feed water is transferred to the head of the pilot following full-scale plant pretreatment, which includes sand filtration, cartridge filtration (5 µm), and sulfuric acid and scale inhibitor addition. Table 2 presents water quality in pilot feed water and total pilot system permeate, collected and analyzed by the University of Central Florida (UCF). Raw water entering the water treatment facility is usually around a pH of 7.1, although sulfuric acid is added as a pretreatment step to lower the pH to 6.5 for hydrogen sulfide and scale control. Conductivity in the feed

water is typically 750 $\mu\text{S}/\text{cm}$, and the total dissolved solids (TDS) concentration in the feed water is around 455 mg/L. Due to the large MWCO of the NF270 membranes, there is no significant removal of monovalent anions and metals; consequently, the typical conductivity and TDS in the pilot permeate are 500 $\mu\text{S}/\text{cm}$ and 250 mg/L, respectively. The organic content of the feed water is typical for a south Florida ground water supply, with a dissolved organic carbon (DOC) concentration of 11 mg/L. The pilot unit removes a substantial portion of organics, with a permeate DOC concentration of <0.25 mg/L.

3.2. Caffeine characterization

Caffeine has frequently been detected in a surficial ground water well that supplies the Town's water treatment facility and nearby irrigation water [43], and does not naturally occur in the environment. Additionally, caffeine was only partially rejected from the total pilot system with a rejection value of 69%, indicating rejection is controlled by diffusion, not size exclusion or electrostatic repulsion. Consequently, caffeine was selected as the TrOC to be modeled.

Caffeine and high performance liquid chromatography (HPLC) grade methanol were purchased from Sigma Aldrich (3300 S. 2nd St., St. Louis, MO). Caffeine properties presented in Table 3 were obtained from Chemicalize.org. The molecular weight of caffeine is 194 g/mole, significantly less than the MWCO of NF270 membranes used in this research. Therefore, the primary rejection mechanism would not be size exclusion. Additionally, caffeine is a neutral compound [35]; consequently, rejection due to electrostatic repulsion would not be plausible. Furthermore, caffeine has an octanol-water partition coefficient ($\text{Log } K_{ow}$) of -0.55 ; therefore, caffeine adsorption to the membrane itself or pilot appurtenances was neither anticipated nor observed.

3.3. Experimental procedure

Experiments were conducted over a course of seven months to obtain enough data to calculate a solute mass

transfer coefficient and create a model, while also obtaining enough data points to validate the model. Table 4 presents the first stage feed caffeine concentrations of 11 experiments ranging from 0.052 to 4,500 $\mu\text{g}/\text{L}$. Although caffeine is not found in water supplies with concentrations near the parts per million level, this wide range of data allowed a more accurate calculation of the caffeine mass transfer coefficient.

3.4. Sample preparation and analytical methods

Samples collected during experiments 1–7 were shipped to and analyzed by a commercial laboratory. Two 40-mL glass amber vials containing 80 μL of 32 g/L sodium omadine (NaOmadine) and 5 mg ascorbic acid were used to collect each sample. Samples were analyzed using a fully automated on-line solid phase extraction, HPLC, mass spectrometry-mass spectrometry system. A detailed description of laboratory methods can be found elsewhere [44].

Samples collected during experiments 8–11 were analyzed by UCF's Civil, Environmental, and Construction Engineering (CECE) and Chemistry Departments; stock solutions of caffeine were prepared in methanol and stored at -20°C . Further dilutions were prepared in water:methanol mixtures (40:60 v/v) and were used as working standard solutions. Water samples were collected in silanized amber bottles and were also prepared in water:methanol mixtures (40:60 v/v) upon returning to UCF laboratories and stored at -20°C until analysis.

Samples were analyzed using a HPLC system. The HPLC experiments were performed using a Perkin-Elmer series 200 HPLC (Santa Clara, CA, USA) consisting of a series 200 binary pump, a series 200 UV-Vis detector with deuterium lamp set at a maximum wavelength of 273 nm, a series 200 autosampler, and a series 200 vacuum degasser. The analytical column used was a Zorbax (Agilent) SB-C18 packed column with a 4.6×150 mm dimensions. The mobile phase was water:methanol 40:60 (v/v) with a flow rate of 1 cm^3/min . Sample run time was 10.0 min with a 10.0- μL injection volume and at isocratic conditions.

Table 3
Caffeine properties


Parameter	Value
Chemical structure	
Classification	Stimulant
Chemical formula	$\text{C}_8\text{H}_{10}\text{N}_4\text{O}_2$
Molecular weight (g/mol)	194
Molecular volume (\AA^3)	164
Polarizability (\AA^3)	179
Octanol-water partition coefficient ($\text{Log } K_{ow}$)	-0.55

Table 4
Caffeine experiment summary

Experiment No.	Feed concentration ($\mu\text{g}/\text{L}$)
1	0.052
2	0.18
3	0.24
4	0.55
5	2.0
6	7.7
7	74
8	1,020
9	1,418
10	2,920
11	4,500

4. Results and discussion

4.1. Model parameter determination

To predict caffeine transport using the HSDM and HSDM-FT, the water mass transfer coefficient, K_w , must be known, as indicated by Eq. (13). Prior to conducting caffeine experiments, K_w was obtained experimentally by operating the pilot unit at various pressures and recording flux changes, then finding the slope of the line generated when water flux was plotted as a function of the net applied pressure, according to Eq. (4). An example of this parameter determination method is represented in Fig. 3 for the total pilot system, and this process was replicated for the first stage and second stage to determine their respective water mass transfer coefficients. A summary of water flux and mass transfer coefficients is presented in Table 5, and coefficient of determination values (R^2) are presented where applicable. The relationship between F_w and K_w , demonstrated in Eq. (5), was used to predict the permeate concentration. The water mass transfer coefficient was 0.667 gsf/d for the total pilot system, and 0.587 and 0.679 gsf/d for the first and second stages of the pilot unit, respectively.

To experimentally determine the caffeine mass transfer coefficient, K_s , experiments were conducted over a wide range of concentrations, as previously presented in Table 4. Average caffeine removal in the first stage, second stage, and total pilot system was 75%, 85%, and 68%, respectively, calculated using Eq. (4). The concentration range of caffeine in the feed during the 11 experiments did not significantly impact rejection, as standard deviations for first stage, second stage, and total

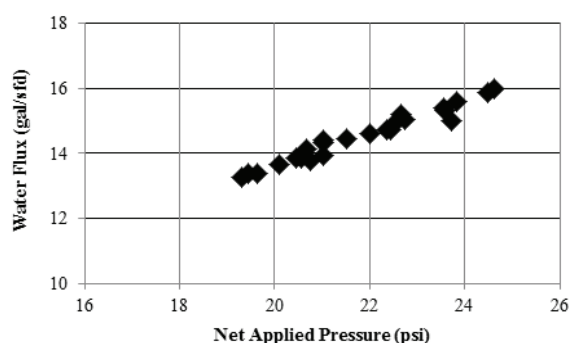


Fig. 3. Total pilot system water flux as a function of net applied pressure.

Table 5
Water flux and water mass transfer coefficients

Stage/ system	Water flux (F_w)		Water mass transfer coefficient (K_w)		
	gsfd	Lmh	gsfd/psi	Lmh/bar	R^2
First stage combined	15.7	26.6	0.667	16.4	0.86
Second stage combined	12.9	21.9	0.587	14.5	0.79
Total pilot system	15.1	26.6	0.679	16.7	0.83

pilot system rejections were 2.6, 5.0, and 2.9, respectively. Similar findings have been demonstrated by others [45,46].

K_s and K_b were both determined experimentally using linear regression. Additionally, K_s was also calculated using Sherwood relationships. To experimentally determine K_s , solute flux values were plotted as a function of the change in caffeine concentrations from the bulk side of the pilot to the total pilot system permeate stream, and the slope of this line was calculated. This methodology was replicated for the first and second stages on both the left and right sides of the pilot to determine their respective caffeine mass transfer coefficients. Furthermore, the same technique was applied to determine K_b values by using Eq. (8). To create and validate a model, 70% of the data was used to create a model, while the remaining 30% of data is used for validation [18]. A total of 52 data points were obtained from first stage, second stage, and the total pilot system. Of these 52 data points, 36 (70%) were used to create the model, while the remaining 16 (30%) were used to validate. Due to the wide range of caffeine feed concentrations, Fig. 4 is presented on a log-scale. The caffeine mass transfer coefficient was determined to be 0.21 ft/d for the total pilot system, while the first stage and second stage caffeine mass transfer coefficients were experimentally determined as 0.32 and 0.27 ft/d, respectively. The caffeine mass transfer coefficients for the first stage left and right sides were 0.31 and 0.27 ft/d, respectively, and 0.25 and 0.26 ft/d for the left and right sides of the second stage, respectively. A summary of experimentally determined caffeine mass transfer coefficients for the first stage, second stage, and total pilot system are presented in Table 6, as well as R^2 values, where applicable. When applying Sherwood relationships, the caffeine mass transfer coefficient was determined to be 2.36 ft/d (8.33×10^{-6} m/s) in the first stage and 2.44 ft/d (8.61×10^{-6} m/s) in the second stage.

4.2. Caffeine prediction and model validation

Flux and mass transfer coefficients presented in Tables 5 and 6 were used in the HSDM and HSDM-FT equations (Eqs. (14) and (15)) to predict the caffeine concentration in the first stage, second stage, and total pilot system permeate, illustrated in Figs. 5, 6, and 7.

Fig. 5 illustrates predicted vs. actual caffeine concentrations in pilot permeate from the total pilot system and from

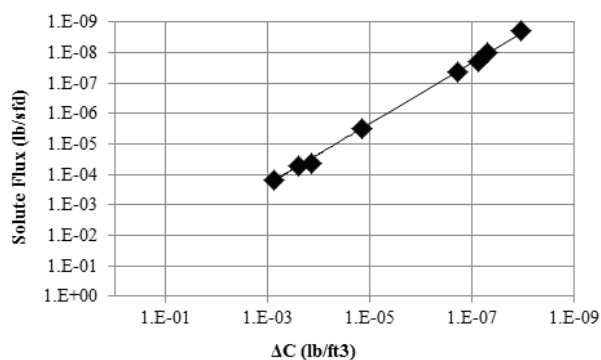


Fig. 4. Total pilot system solute flux as a function of change in caffeine concentration.

Table 6
Caffeine mass transfer coefficients

Stage/system	Mass transfer coefficient (K_s)			$\exp\left(\frac{F_w}{k_b}\right)$		Back-transport mass transfer coefficient (k_b)	
	ft/d	m/s	R^2	Unitless	R^2	ft/d	m/s
First stage combined	0.32	1.1×10^{-6}	1.0	2.44	1.0	2.35	8.3×10^{-6}
First stage left	0.31	1.1×10^{-6}	0.99	2.11	1.0	2.80	9.9×10^{-6}
First stage right	0.27	9.6×10^{-7}	0.99	2.06	1.0	2.87	1.0×10^{-5}
Second stage combined	0.27	9.6×10^{-7}	0.99	1.55	1.0	3.95	1.4×10^{-5}
Second stage left	0.25	8.8×10^{-7}	1.0	1.45	1.0	4.68	1.7×10^{-5}
Second stage right	0.26	9.3×10^{-7}	1.0	1.52	1.0	3.99	1.4×10^{-5}
Total pilot system	0.21	7.6×10^{-7}	0.99	3.72	1.0	1.54	5.4×10^{-6}

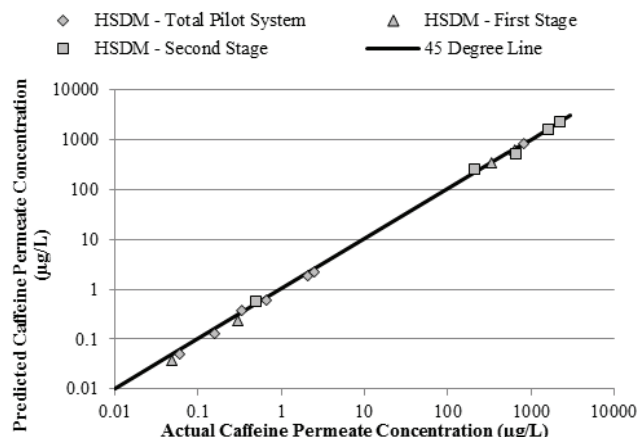


Fig. 5. Predicted vs. actual caffeine concentration from first stage, second stage, and total pilot system permeate using the HSDM at low and high feed concentrations. Results are plotted on a log-scale due to the wide range of concentrations.

the left and right sides of stages 1 and 2 using the HSDM. Results are plotted on a log-scale due to the wide range of permeate concentrations and represent a total of 16 data points. The solid 45° line represents a plot of predicted vs. actual caffeine if there was no model error. Model verification was determined by conducting a paired *t*-test on predicted and actual caffeine data. Based on the paired *t*-test and the predicted vs. actual caffeine concentrations demonstrated in Fig. 5, it appears that experimentally derived caffeine mass transfer coefficients used in the HSDM are successful in predicting caffeine concentrations in the first stage, second stage, and total pilot system permeate. The average relative percentage difference (RPD) of predicted and actual caffeine concentrations in the permeate streams was 12%.

Figs. 6 and 7 represent predicted vs. actual permeate concentration using the HSDM and HSDM-FT, at low and high feed concentrations, respectively. The HSDM-FT slightly over-predicts caffeine in the permeate streams, indicating concentration polarization does not significantly affect caffeine permeation through this NF pilot. This could be due

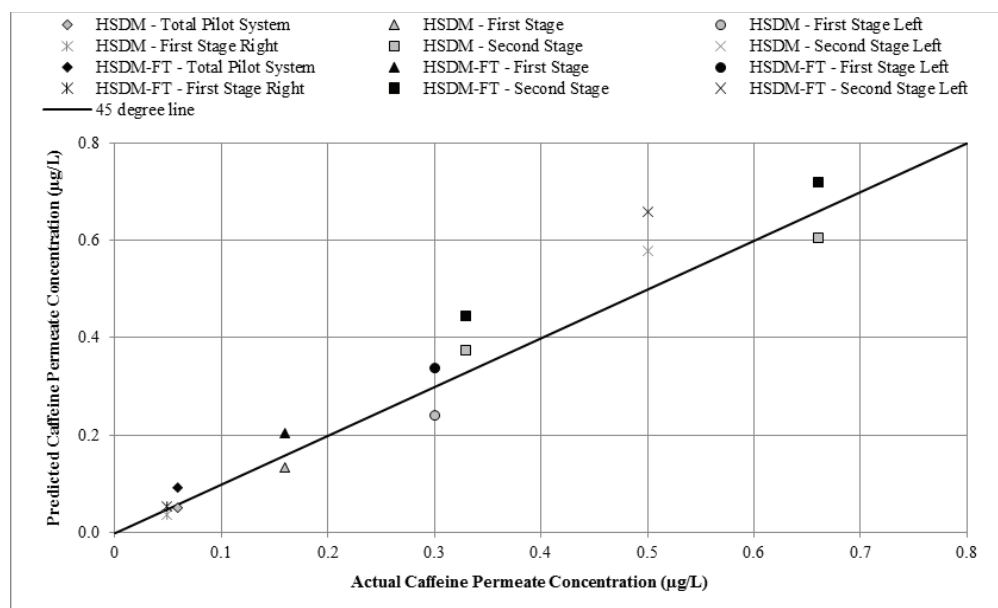


Fig. 6. Predicted vs. actual caffeine concentration from first stage, second stage, and total pilot system permeate using the HSDM and HSDM-FT at low feed concentrations.

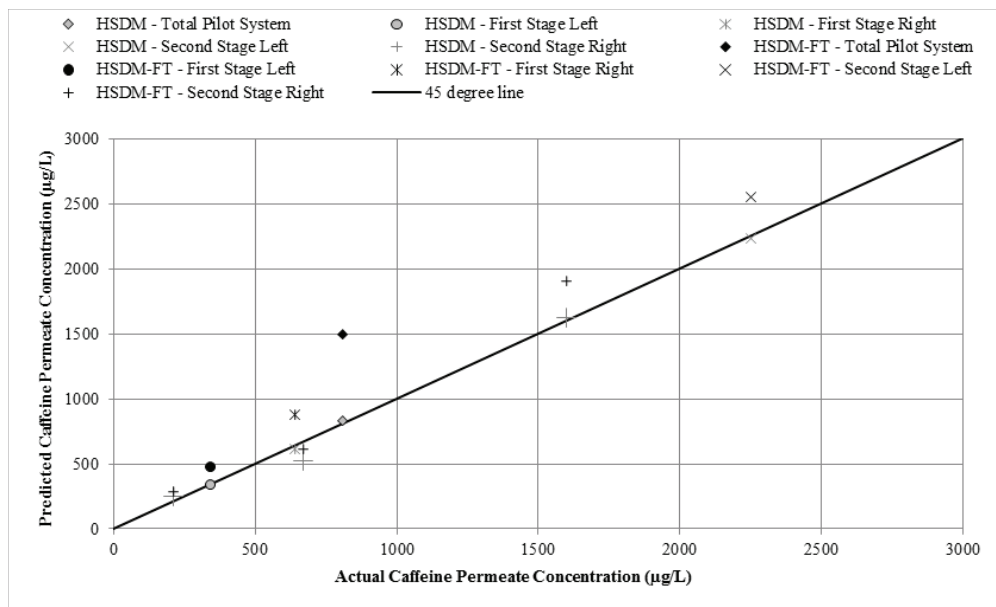


Fig. 7. Predicted vs. actual caffeine concentration from first stage, second stage, and total pilot system permeate using the HSDM and HSDM-FT at high feed concentrations.

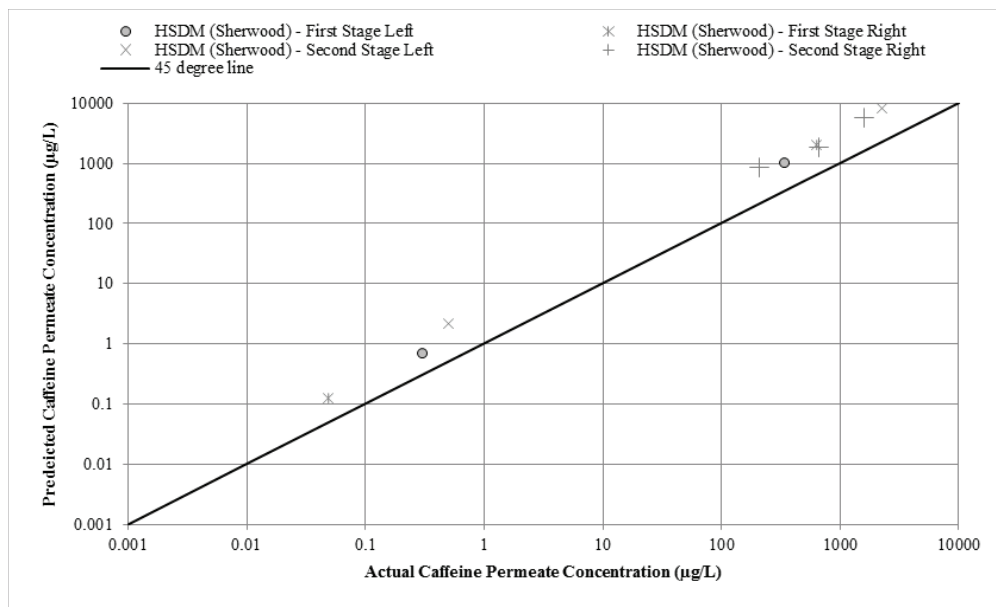


Fig. 8. Predicted vs. actual caffeine concentration in permeate from left and right sides of first and second stages of pilot system using the HSDM with the mass transfer coefficients calculated using Sherwood relationships.

to the low operating pressure and high feed flow rate of the pilot unit. These findings are similar to those found by Zhao et al. [25]. When compared with the HSDM, the HSDM-FT is not as accurate in predicting the caffeine concentration in permeate, as the RPD between predicted and actual caffeine concentrations was 27% and the paired *t*-test indicated a statistically significant difference between predicted and actual caffeine concentrations in permeate streams.

When calculated using Sherwood relationships, the mass transfer coefficients appear to over-predict caffeine concentration in the permeate streams, as demonstrated on

a log-scale in Fig. 8. Fig. 8 presents data from the left and right sides of first and second stages of the pilot system, and the RPD between predicted and actual caffeine concentrations in permeate streams was 104%. Additionally, a paired *t*-test revealed a statistically significant difference between predicted and actual caffeine concentrations. This over-prediction could be due to a variety of reasons that include the possibility of Wilke-Chang coefficients used in Eq. (12) may be too conservative as well as field conditions. Alternatively, this method could have over-predicted caffeine transport since Sherwood correlations do not strongly

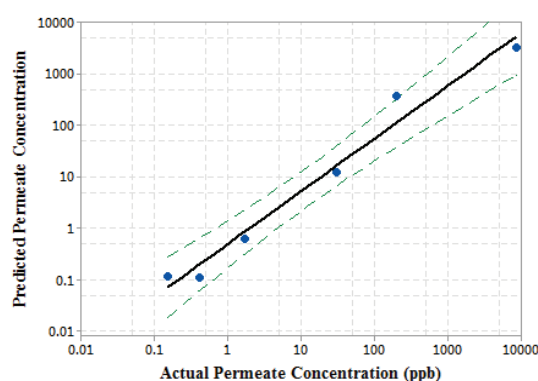


Fig. 9. Predicted caffeine concentration vs. actual caffeine concentration in permeate using results found in the literature.

consider caffeine or water properties [4,40]. Others have demonstrated similar findings, where models over-predict TDS mass transfer at low TDS concentrations [25] similar to what was experienced in the pilot study.

Fig. 9 was generated using Minitab® and illustrates predicted permeate concentrations obtained using the HSDM and mass transfer coefficients presented in Table 6, vs. actual permeate concentrations using results obtained using data from outside literature sources [6,47–51]. Fig. 9 is plotted on a log-scale due to the wide range of concentrations. The dashed lines represent 95% confidence bands, and the solid line represents the trend line between predicted and actual permeate concentrations. Feed and permeate caffeine concentrations from outside literature data range from 1 to 11,250 $\mu\text{g}/\text{L}$ and 0.15 to 8,600 $\mu\text{g}/\text{L}$, respectively. Predicted permeate caffeine concentrations were calculated using operating data from the literature sources. Sources range from loose NF to RO membranes, and rejection of caffeine ranges from 24% to 85%. Results indicate that the HSDM and experimentally derived caffeine mass transfer coefficients were able to predict the caffeine concentration in the permeate samples from the six outside literature sources.

5. Conclusions

This work investigated the caffeine removal efficiency of an NF membrane process at the pilot-scale and established mass transfer models for water and caffeine transport using two diffusion-based models: the solution diffusion model and the solution diffusion model with FT. Experiments were carried out using a 267-gpm, split-feed, center-exit NF pilot operating as a two-stage system that utilizes a surficial groundwater source. Caffeine concentrations ranging from 0.052 to 4,500 $\mu\text{g}/\text{L}$ were used in the feed water, and the average caffeine removal efficiency from the total pilot system was 68%, with rejections of 75% and 85% in the first and second stages, respectively. Removal did not vary by solute concentration for constant flux ($25.6 \text{ L m}^{-2} \text{ h}^{-1}$) and temperature (25°C) operating conditions.

Mass transfer models evaluated in this work include the HSDM with and without FT, in addition to dimensional analysis, using the Sherwood number, and were shown to predict NF solute mass transfer. The models were validated to within a 95% confidence interval using a combination

of results reported in this research and data obtained from independent literature sources. Predicted vs. actual caffeine content was linearly compared, revealing correlation coefficients on the order of 0.99, 0.96, and 0.99 for the HSDM without FT, HSDM-FT, and the Sherwood number, respectively. However, the use of the HSDM-FT and the Sherwood number resulted in the over-prediction of caffeine concentrations in permeate streams by 27% and 104%, respectively.

Acknowledgments

The work reported herein was funded by UCF project agreement number 16208114. The authors acknowledge the Town's utilities staff, including David Brown, Amanda Barnes, Paul Jurczak, and Rebecca Wilder, for their assistance and support, without whom this work would not have been possible. The authors also acknowledge the consultation and advice of Ian Watson (RosTek Associates Inc.) and John Potts (Kimley-Horn & Associates, Inc.). Additional thanks are offered to the UCF graduate and undergraduate students who assisted in this work.

References

- [1] K.K. Barnes, D.W. Kolpin, E.T. Furlong, S.D. Zaugg, M.T. Meyer, L.B. Barber, A national reconnaissance of pharmaceuticals and other organic wastewater contaminants in the United States – I) Groundwater, *Sci. Total Environ.*, 402 (2008) 192–200.
- [2] D.W. Kolpin, E.T. Furlong, M.T. Meyer, E.M. Thurman, S.D. Zaugg, L.B. Barber, H.T. Buxton, Pharmaceuticals, hormones, and other organic wastewater contaminants in U.S. Streams, 1999–2000: a national reconnaissance, *Environ. Sci. Technol.*, 36 (2002) 1202–1211.
- [3] M.J. Focazio, D.W. Kolpin, K.K. Barnes, E.T. Furlong, M.T. Meyer, S.D. Zaugg, B. Barber, M.E. Thurman, A national reconnaissance for pharmaceuticals and other organic wastewater contaminants in the United States – II) Untreated drinking water sources, *Sci. Total Environ.*, 402 (2008) 201–216.
- [4] S.J. Duranceau, J.S. Taylor, L.A. Mulford, SOC removal in a membrane softening process, *J. Amer. Water Works Assoc.*, 84:1 (1992) 68–78.
- [5] P. Xu, J.E. Drewes, C. Bellona, G. Amy, T.-U. Kim, M. Adam, T. Heberer, Rejection of emerging organic micropollutants in nanofiltration-reverse osmosis membrane applications, *Water Environ. Res.*, 77 (2005) 40–48.
- [6] C. Bellona, J.E. Drewes, Viability of a low-pressure nanofilter in treating recycled water for water reuse applications: a pilot-scale study, *Water Res.*, 41 (2007) 3948–3958.
- [7] J. Radjenovic, M. Petrovic, F. Ventura, D. Barcelo, Rejection of pharmaceuticals in nanofiltration and reverse osmosis membrane drinking water treatment, *Water Res.*, 42 (2008) 3601–3610.
- [8] V. Yangali-Quintanilla, S.K. Maeng, T. Fujioka, M. Kennedy, Z. Li, G. Amy, Nanofiltration vs. reverse osmosis for the removal of emerging organic contaminants in water reuse, *Desal. Wat. Treat.*, 34 (2011) 50–56.
- [9] C. Bellona, J. Drewes, P. Xu, G. Amy, Factors affecting the rejection of organic solutes during NF/RO treatment – a literature review, *Water Res.*, 38 (2004) 3795–2809.
- [10] A.M. Comerton, R.C. Andrews, D.M. Bagley, The influence of natural organic matter and cations on the rejection of endocrine disrupting and pharmaceutically active compounds by nanofiltration, *Water Res.*, 43 (2009) 613–622.
- [11] V. Yangali-Quintanilla, A. Sadmani, M. McConville, M. Kennedy, G. Amy, Rejection of pharmaceutically active compounds and endocrine disrupting compounds by clean and fouled nanofiltration membranes, *Water Res.*, 43 (2009) 2349–2362.

- [12] Y.-L. Lin, C.-H. Lee, Elucidating the rejection mechanisms of PPCPs by nanofiltration and reverse osmosis membranes, *Ind. Eng. Chem. Res.*, 53 (2014) 6798–6806.
- [13] J. Lin, C.Y. Tang, C. Huang, Y.P. Tang, W. Ye, J. Li, J. Shen, R. Van de Broeck, J. Van Impe, A. Volodin, C. Van Haesendonck, A. Sotto, P. Luis, B. Van der Bruggen, A comprehensive physico-chemical characterization of superhydrophilic loose nanofiltration membranes, *J. Membr. Sci.*, 501 (2016) 1–14.
- [14] J. Lin, W. Ye, H. Zeng, H. Yang, J. Shen, S. Darvishmanesh, P. Luis, A. Sotto, B. Van der Bruggen, Fractionation of direct dyes and salts in aqueous solution using loose nanofiltration membranes, *J. Membr. Sci.*, 477 (2015) 183–193.
- [15] J. Lin, C.Y. Tang, W. Ye, S.-P. Sun, S.H. Hamdan, A. Volodin, C. Van Haesendonck, A. Sotto, P. Luis, B. Van der Bruggen, Unraveling flux behavior of superhydrophilic loose nanofiltration membranes during textile wastewater treatment, *J. Membr. Sci.*, 493 (2015) 690–702.
- [16] R. Schlögl, Membrane permeate in system far from equilibrium, *Ber Bunsenges. Phys. Chem.*, 70 (1996) 400–414.
- [17] W.R. Bowen, A.W. Mohammad, N. Hilal, Characterisation of nanofiltration membranes for predicted purposes – use of salts, uncharged solutes and atomic force microscopy, *J. Membr. Sci.*, 126 (1997) 91–105.
- [18] D. Vezzani, S. Bandini, Donnan equilibrium and dielectric exclusion for characterization of nanofiltration membranes, *Desalination*, 149 (2002) 477–483.
- [19] A.W. Mohammad, Y.H. Teow, W.L. Ang, Y.T. Chung, D.L. Oatley-Radcliffe, N. Hilal, Nanofiltration membranes review: recent advances and future prospects, *Desalination*, 356 (2015) 226–254.
- [20] T. Chaabane, S. Taha, M. Taleb Ahmed, R. Maachi, G. Dorange, Coupled model of film theory and the Nernst-Planck equation in nanofiltration, *Desalination*, 206 (2007) 424–432.
- [21] S. Bandini, D. Vezzani, Nanofiltration modeling: the role of dielectric exclusion in membrane characterization, *Chem. Eng. Sci.*, 58 (2003) 3303–3326.
- [22] X.-m. Wang, B. Li, T. Zhang, X.-y. Li, Performance of nanofiltration membrane in rejecting trace organic compounds: experiment and model prediction, *Desalination*, 370 (2015) 7–16.
- [23] F.-x. Kong, H.-w. Yang, X.-m. Wang, Y.F. Xie, Assessment of the hindered transport model in predicting the rejection of trace organic compounds by nanofiltration, *J. Membr. Sci.*, 498 (2016) 57–66.
- [24] Y. Zhao, J.S. Taylor, Modeling membrane performance over time, *J. Am. Water Works Assoc.*, 96 (2004) 90–97.
- [25] Y. Zhao, J.S. Taylor, S. Chellam, Predicting RO/NF water quality by modified solution diffusion model and artificial neural networks, *J. Membr. Sci.*, 263 (2005) 38–46.
- [26] L.-Y. Hung, S.J. Lue, J.-H. You, Mass-transfer modeling of reverse-osmosis performance on 0.5–2% salty water, *Desalination*, 265 (2011) 67–73.
- [27] A.R.D. Verliefde, E.R. Cornelissen, S.G.J. Heijman, J.Q.J.C. Verberk, G.L. Amy, B. Van der Bruggen, J.C. van Dijk, Construction and validation of a full-scale model for rejection of organic micropollutants by NF membranes, *J. Membr. Sci.*, 339 (2009) 10–20.
- [28] A.M. Hidalgo, G. Leon, M. Gomez, M.D. Murcia, D.S. Barbosa, P. Blanco, Application of the solution-diffusion model for the removal of atrazine using a nanofiltration membrane, *Desal. Wat. Treat.*, 51 (2012) 2244–2252.
- [29] A.M. Hidalgo, G. Leon, M. Gomez, M.D. Murcia, E. Gomez, J.L. Gomez, Modeling of aniline removal by reverse osmosis using different membranes, *Chem. Eng. Technol.*, 34 (2011) 1753–1759.
- [30] J.G. Wijmans, R.W. Baker, The solution-diffusion model: a review, *J. Membr. Sci.*, 107 (1995) 1–21.
- [31] A.M.F. Shaaban, A.I. Hafez, M.A. Abdel-Fatah, N.M. Abdel-Monem, M.H. Mahmoud, Process engineering optimization of nanofiltration unit for the treatment of textile plant effluent in view of solution diffusion model, *Egypt. J. Pet.*, 25 (2016) 79–90.
- [32] J. Wang, D.S. Dlamini, A.K. Kishra, M.T.M. Pendergast, M.C.Y. Wong, B.B. Mamba, V. Freger, A.R.D. Verliefde, E.M.V. Hoek, A critical review of transport through osmotic membranes, *J. Membr. Sci.*, 454 (2014) 516–537.
- [33] American Water Works Association (AWWA), *Manual of Water Supply Practices – M46: Reverse Osmosis and Nanofiltration*, 2nd ed., American Water Works Association, Colorado, 2007.
- [34] Z.V.P. Murthy, S.K. Gupta, Estimation of mass transfer coefficient using a combined nonlinear membrane transport and film theory model, *Desalination*, 109 (1997) 39–49.
- [35] A.R.D. Verliefde, E.R. Cornelissen, S.G.J. Heijman, J.Q.J.C. Verberk, G.L. Amy, B. Van der Bruggen, J.C. van Dijk, Construction and validation of a full-scale model for the rejection of organic micropollutants by NF membranes, *J. Membr. Sci.*, 339 (2009) 10–20.
- [36] C.R. Wilke, P. Chang, Correlations of diffusion coefficients in dilute solutions, *AIChE J.*, 1 (1955) 264–270.
- [37] T.K. Sherwood, P.L.T. Brian, R.E. Fisher, *Desalination by reverse osmosis*, *Ind. Eng. Chem. Fundam.*, 6 (1967) 2–12.
- [38] W.H. Linton, T.K. Sherwood, Mass transfer from solids shapes to water in streamline and turbulent flow, *Chem. Eng. Prog.*, 46 (1950) 258–264.
- [39] S. Lee, G. Amy, J. Cho, Applicability of Sherwood correlations for natural organic matter (NOM) transport in nanofiltration (NF) membranes, *J. Membr. Sci.*, 240 (2004) 49–65.
- [40] S. Chellam, J.S. Taylor, Simplified analysis of contaminant rejection during ground- and surface water nanofiltration under the information collection rule, *Water Res.*, 35 (2001) 2460–2474.
- [41] L.D. Nghiem, A.I. Schafer, M. Elimelech, Removal of natural hormones by nanofiltration membranes: measurement, modeling, and mechanisms, *Environ. Sci. Technol.*, 38 (2004) 1888–1896.
- [42] C. Bellona, D. Heil, C. Yu, P. Fu, J.E. Drewes, The pros and cons of using nanofiltration in lieu of reverse osmosis for indirect potable reuse applications, *Sep. Purif. Technol.*, 85 (2012) 69–76.
- [43] R.J. Wilder, S.J. Duranceau, S. Jeffery, D. Brown, A. Arrington, Contaminants of Emerging Concern: Occurrence in Shallow Groundwater and Removal by Nanofiltration, *Proc. American Membrane Technology Association Conference*, San Antonio, TX, 2016.
- [44] J. Oppenheimer, A. Eaton, M. Badruzzaman, A.W. Haghani, J.G. Jacangelo, Occurrence and suitability of sucralose as an indicator compound of wastewater loading to surface waters in urbanized regions, *Water Res.*, 45 (2011) 4019–4027.
- [45] A. Bodalo, G. Leon, A.M. Hidalgo, M. Gomez, M.D. Murcia, P. Blanco, Atrazine removal from aqueous solutions by nanofiltration, *Desal. Wat. Treat.*, 13 (2010) 143–148.
- [46] Y. Zhang, B. Van der Bruggen, G.X. Chen, L. Braeken, C. Vandecasteele, Removal of pesticides by nanofiltration: effect of the water matrix, *Sep. Purif. Technol.*, 38 (2004) 163–172.
- [47] K. Kimura, S. Toshima, G. Amy, Y. Watanabe, Rejection of neutral endocrine disrupting compounds (EDCs) and pharmaceutical active compounds (PhACs) by RO membranes, *J. Membr. Sci.*, 245 (2004) 71–78.
- [48] A.M. Comerton, R.C. Andrews, D.M. Bagley, C. Hao, The rejection of endocrine disrupting and pharmaceutically active compounds by NF and RO membranes as a function of compound and water matrix properties, *J. Membr. Sci.*, 313 (2008) 323–335.
- [49] N. Garcia-Vaquero, E. Lee, J. Castaneda, J. Cho, J.A. Lopez-Ramirez, Comparison of drinking water pollutant removal using a nanofiltration pilot plant powered by renewable energy and a conventional treatment facility, *Desalination*, 347 (2014) 94–102.
- [50] V. Yangali-Quintanilla, S.K. Maeng, T. Fujioka, M. Kennedy, G. Amy, Proposing nanofiltration as acceptable barrier for organic contaminants in water reuse, *J. Membr. Sci.*, 362 (2010) 334–345.
- [51] A. Shahmansouri, C. Bellona, Application of quantitative structure-property relationships (QSPRs) to predict the rejection of organic solutes by nanofiltration, *Sep. Purif. Technol.*, 118 (2013) 627–638.